JOURNAL OF THEORETICAL AND APPLIED MECHANICS
62, 3, pp. 587-599, Warsaw 2024
https://doi.org/10.15632/jtam-pl/191444

EVALUATION OF MICROSTRUCTURE AND MECHANICAL PROPERTIES OF FERROMAGNETIC STRUCTURAL STEELS USING BARKHAUSEN NOISE

Katarzyna Makowska
Military University of Technology, Faculty of Mechatronics, Armament and Aerospace, Warsaw, Poland
corresponding author, e-mail: katarzyna.makowska@wat.edu.pl
Zbigniew L. Kowalewski
Institute of Fundamental Technological Research of the Polish Academy of Sciences, Warsaw, Poland
e-mail: zkowalew@ippt.pan.pl

The paper presents an attempt to assess the microstructure and mechanical properties by means of the magnetic Barkhausen noise (MBN) method. The experimental program was supplemented by metallographic examinations and hardness tests. It has been concluded that the MBN method can be used for non-destructive characterization of both single and two-phase steels used in the automotive industry. It was also found that the microstructure of steel can be distinguished using the shape of BN envelope and two magnetic parameters: $U_{b_{pp1}}$ and U_{g1}. On the other hand, the hardness and ultimate tensile strength are described successfully by the $U_{g1}/U_{b_{pp1}}$ parameter.

Keywords: microstructure, mechanical properties, Barkhausen noise, non-destructive method

1. Introduction

Magnetic Barkhausen Noise (MBN) analysis (Jiles, 1998) is regarded as a non-destructive technique of considerable significance in microstructural characterization of ferromagnetic materials. Contemporary industrial requirements enforce research work for effective determination and better assurance of the desired microstructure of steels. In practice, the microstructure is determined by selected metallographic techniques and hardness tests where certain regions of representative specimens can be taken into account. Since application of these methods is time consuming and quite expensive, there is an interest to develop cheap non-destructive techniques capable of rapid inspection of the material state. Performing BN measurements instead of metallographic and hardness tests may reduce the cost of quality control while maintaining its standards.

Among many options, the MBN method can be applied to detect and determine a volume of the sigma phase in duplex stainless steels (Huallpa *et al.*, 2016). Since the sigma phase adversely affects mechanical properties and corrosion resistance of the material, it is necessary to determine its contribution. It has been shown, that a volume of the sigma phase increases as the time of annealing increases (Huallpa *et al.*, 2016). Simultaneously, the BN signal decreases until it equalizes the background level after 24 hours of heat treatment (Huallpa *et al.*, 2016).

Singh *et al.* (2020) showed, that the MBN gets an effective opportunity to distinguish between such thermal treatments as annealing, normalization and quenching. Three variants of heat treatment were carried out. The annealing, normalizing and quenching processes were carried out alternatively at 900°C, 850°C and 800°C. The highest level of the BN signal was obtained for the material annealed at 900°C, and then, successively for the material annealed at 850°C and 800°C. Lower values of BN signal were measured on specimens after normalization. The same tendency of the BN signald variation due to temperature change was observed. The lowest

values of BN were obtained for specimens after quenching, however, an opposite trend was noted, i.e. the highest BN was observed for the specimen thermally treated at 800°C, and the lowest one for 900°C. However, Honkanen *et al.* (2021) stated that based only on the BN amplitude, the ferritic-pearlitic and martensitic microstructure could not be distinguished.

The bainite fraction in 22MnB5 grade steel with 0.23%C was also tested by means of the MBN method (Zhu *et al.*, 2020). Specimens of different bainite and martensite contributions were produced and, subsequently, the peak of MBN and rms value were analysed. A decrease in the BN was observed for the bainite volume lower than 30%. Above this volume, an increase of MBN was noted. The residual internal stresses in the martensite phase were the main reasons of the BN decrease.

According to (Błażewski and Mikoszewski, 1981), an increase of BN due to the bainite fraction increase can be attributed to a lower resistance of the domain walls during the magnetisation cycle in comparison to the small lath structure of martensite with high dislocation density (Kaplan *et al.*, 2007).

A content of the martensitic phase in X70 dual-phase steel after various heat treatments of different inter-critical annealing temperature was tested in (Nebair *et al.*, 2022). It was found that BN decreases if the inter-critical temperature increases. This is due to an increase of the martensite fraction and the number of obstacles as well (Nebair *et al.*, 2022).

In (Tavares *et al.*, 2019) temper embrittlements contributions were detected in the supermartensitic stainless SMSS steel (13%Cr-5%Ni-2%Mo) by MBN. This material belongs to the class of new stainless steels developed in the 1990's. It is commonly used for production of seamless pipes and forged parts for oil and gas installations on land. Conventional martensitic stainless steels become brittle when tempered in the temperature range of 400°C-600°C, as can be verified by impact Charpy tests at room temperature (Pickering, 1976).

Nowadays, the MBN is used as a standard to evaluate the tempering process of steel (Ivanova, 2022). It was found that the time of noise registration could serve as a suitable parameter for analysis of the microstructure. It can be determined on the basis of the zero point of the magnetization sine wave and maximum value of the magnetic noise envelope (Ivanova, 2022). The study found linear relationships between the time of magnetic noise occurrence and the hardness of structures obtained after tempering. The same nature of the relationship was found between the hardness of heat treated structures and the rms signal of BN (Ivanova, 2022).

In (Neslušan *et al.*, 2023), the Barkhausen emission was used to distinguish steels of different yield strengths: 355 MPa, 500 MPa, 700 MPa, 960 MPa and 1100 MPa. It was observed that for specimens investigated non-destructively along the sheet rolling direction, firstly, the BN signal increased up to about 500 MPa, subsequently, it was approximately constant up to about 1000 MPa, and finally decreased. On the contrary, in the case of specimens investigated by means of MBN method in the transverse direction, the BN increased up to 1000 MPa, and then decreased (Neslušan *et al.*, 2023).

Astudillo *et al.* (2022) used the BN to detect presence of martensite induced by deformation. A progressive increase of the rms value of the MBN with an increase of martensite volume was verified (Astudillo *et al.*, 2022). The results showed that the MBN might detect microstructural changes that occurred during the evaluation of initiation and evolution of the austenite–martensite phase transformation (Astudillo *et al.*, 2022). The presented literature examples indicate that the MBN can be useful for identification of the steel microstructure.

Based on this short survey of the BN studies, one can conclude that the method is suitable in many materials science issues. What is lacking, however, is a synthetic description of the microstructure evaluated by means of MBN for a wide range of structural steel grades, commonly used in major industrial branches. Moreover, the available literature data shows that there are no clear answers to rhe question, which parameters determined from the BN envelope allow one

to precisely identify the type of microstructures. This research is an attempt to get closer to answering this question.

2. Experimental procedure

Six structural steels were taken from different automotive or military components (Mars 300 – protective armour fragment – Specimen No. 1), 40NiCrMo7 – ball pin – Specimen No. 2), S700MC – boom toa of a special truck – Specimen No. 3, S355 steel – car trailer – Specimen No. 4, C55 – ball joint housing – Specimen No. 5, and C15 – car stick – Specimen No. 6). Chemical compositions of the tested steels are presented in Table 1.

Table 1. Chemical compositions of the tested steel grades

No.	Steel grade	C	S	P	Si	Mn	Ni	Cr	Mo	V	S	Al	Ti
1	Mars 300	0.49	0.001	0.005	1.01	0.60	1.70	0.30	0.40	–	–	–	–
2	40NiCrMo7	0.38	0.020	0.010	0.26	0.62	1.35	0.82	0.23	–	–	–	–
3	S700MC	0.11	0.013	0.012	0.30	1.87	–	–	0.31	0.10	0.003	0.012	0.21
4	C55	0.56	0.034	0.021	0.23	0.72	0.24	0.38	0.02	–	–	–	–
5	S355	0.09	0.012	0.023	0.47	1.63	–	–	0.40	0.20	0.004	0.013	0.19
6	C15	0.13	0.014	0.022	0.18	0.45	–	–	–	–	–	–	–

Non-destructive Barkhausen tests as well as metallographic and hardness tests were performed on them. Subsequently, a mutual relationship between magnetic properties and the microstructure type of structural steel were found. The surfaces of the elements on which the tests were carried out were polished with a sandpaper with grains of 320 and 1200.

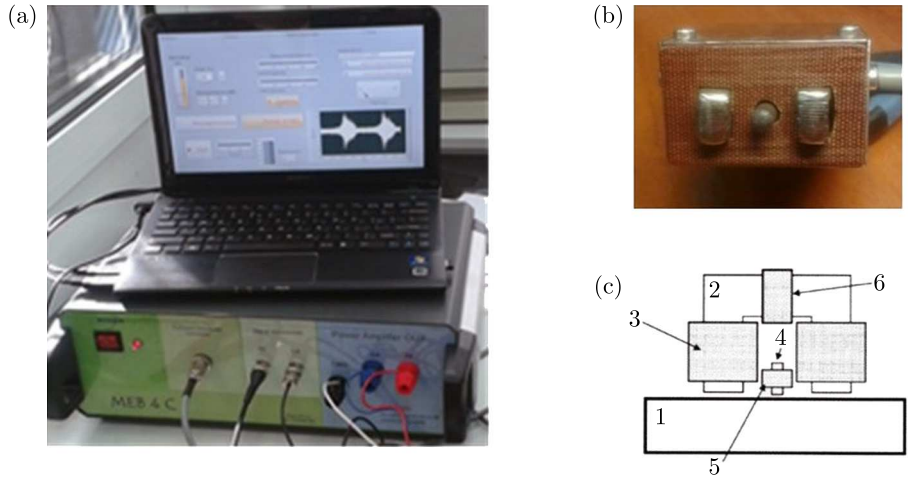

Fig. 1. Barkhausen noise defectoscope: (a) general view, (b) head, (c) diagram of the head (1 – tested specimen, 2 – U-shaped core, 3 – magnetising coil, 4 – core of the measuring coil, 5 – measuring winding, 6 – control winding) (Makowska and Kowalewski, 2020)

Magnetic tests were carried out using the Barkhausen noise defectoscope, Fig. 1. Three measurements were carried out in one area of each specimen. Barkhausen noise envelopes with the highest amplitude are shown. The sensor was set in accordance with the rolling direction of the materials in question. The measuring head consisted of a U-shaped core of electromagnets wrapped in a wound excitation coil. The pick-up coil was built into the sensor that possessed a rounded shape which made it easier to fit the probe to concave and convex surfaces. The control coil was also built into the head. The voltage of the control coil reached its maximum

value when the probe was optimally positioned on the specimen. The voltage signal induced in the coil was proportional to the rate of change of the magnetic flux in the electromagnet core (Makowska and Kowalewski, 2020). The size of the magnetic flux depends on its surface and the magnetic properties of both the core and object tested (Makowska and Kowalewski, 2020). The detailed structure of the sensor is presented on Fig. 1c. A triangular waveform was applied. In the pick-up coil, a voltage signal U_0 was induced. In order to estimate the BN intensity, the fast-variable component of U_0 was measured for the frequency $f = (0-500)$ Hz. Analysis of this component provided required data on the material structure of the specimen.

The envelopes of BN were calculated as rms value of U_b according to

$$U_b = \sqrt{\frac{1}{\tau}\int_0^{\tau} U_{tb1}^2(t)\,dt} \tag{2.1}$$

where U_b [V] is the root mean square of the coil output voltage; U_{tb1} [V] is the fast-variable component defining a voltage separated by means of the high-pass filter from induced voltage in the pick-up coil, and τ [s] is the integration time.

In the next step, the amplitude of BN (Ub_{pp}) was used as a parameter defining the voltage difference between the maximum peak value of the MBN (U_b) and the background noise (U_{tb}). The MBN amplitude is able to identify the BN level that depends on microstructural features of the material matrix like the grain boundaries, precipitations or dislocations for example. Also a voltage generator U_g was determined for each Ub_{pp} value. It gives information on the magnetic field strength that is needed to overcome pinning obstacles by the domain walls (Makowska and Kowalewski, 2020).

Also, an integral of the half-period voltage signal of MBN was calculated

$$Int(Ub) = \int_{-U_{g_{max}}}^{+U_{g_{max}}} U_{sb}\,dU_g \tag{2.2}$$

where

$$U_{sb} = \sqrt{U_b^2 - U_{tb}^2} \tag{2.3}$$

and U_{sb} [V] – root mean square of the Barkhausen emission voltage after correction due to background noise, U_b [V] – root mean square of the coil output voltage, U_{tb} [V] – root mean square of background voltage, U_g [V] – generator voltage.

The full width of the half maximum FWHM was also determined. It can be related to the magnetic hardness (Jiles, 1998). In the case of two maxima on the envelope, the amplitude and integral were determined for the following parameters: $U_{b_{pp1}}$, $U_{b_{pp2}}$, $Int(Ub)_1$, $Int(Ub)_2$, $FWHM_1$ and $FWHM_2$. Also, the new $U_{g1}/U_{b_{pp1}}$ parameter was calculated.

The microstructure of the tested materials was analysed using the Olympus PMG 3 light microscope equipped in Zen2Core software. Quantitative analysis of the microstructure was performed using the linear method. The longest chord, also called the Ferret diameter, was proposed as the grain size parameter d_{av} [μm]. The following notations were adopted in this work: $d_{av\,(M)}$ – average grain size of martensite, $d_{av\,(S)}$ – average grain size of high-tempered martensite (sorbite), $d_{av\,(B)}$ – average grain size of bainite, $d_{av\,(F)}$ – average grain size of ferrite, $d_{av\,(P)}$ – average grain size of pearlite, $d_{av\,(C)}$ – average grain size of cementite, V_F – volume fraction of ferrite, V_P – volume fraction of pearlite, V_C – volume fraction of cementite. A relationship between the grain size and amplitude of Barkhausen noise was found.

The Vickers hardness (HV 3) was measured by means of the universal Duramin-500 Struers hardness tester. Five measurements were carried out for each specimen. The Vickers hardness values were converted into the Brinell hardness (Błażewski and Mikoszewski, 1981) in order to assess the ultimate tensile stress, Table 2.

Table 2. Hardness results of the steel grades tested

Steel grade [HV3]	Mars 300	40NiCrMo7	S700MC	C55	S355	C15
Measurement 1	708	306	252	208	165	158
Measurement 2	696	297	258	216	163	156
Measurement 3	705	301	250	212	162	155
Measurement 4	704	308	262	210	168	159
Measurement 5	701	296	260	214	166	157
Average hardness	703	302	256	212	165	157
Standard deviation	±4.07	±4.76	±4.63	±2.83	±2.14	±1.41

3. Results

The envelopes of BN are presented in Fig. 2, whereas the parameters coming from BN envelopes are shown in Figs. 3-6. Microstructures of the tested materials are presented in Fig. 7.

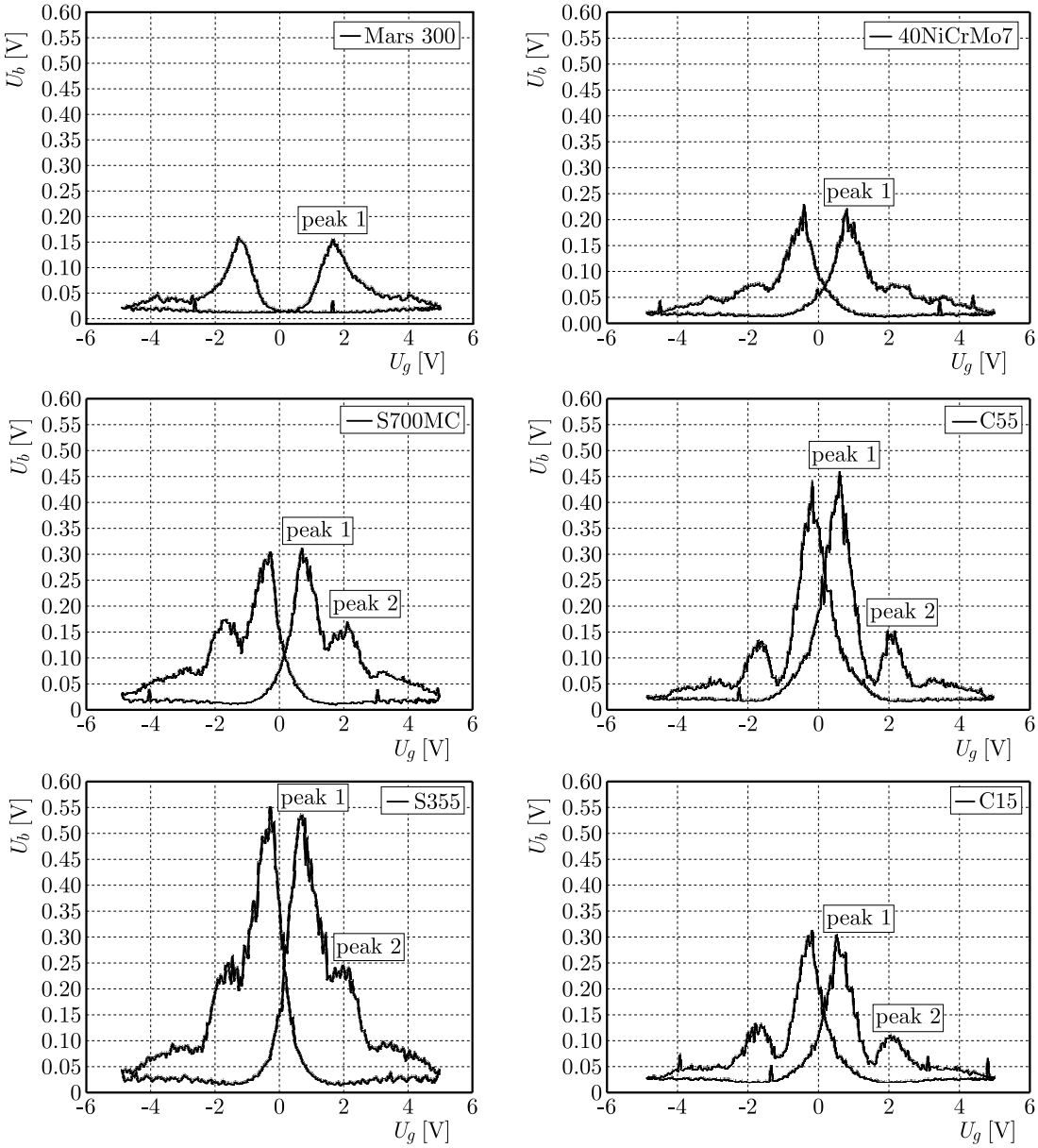

Fig. 2. Barkhausen noise envelopes for different steel grades

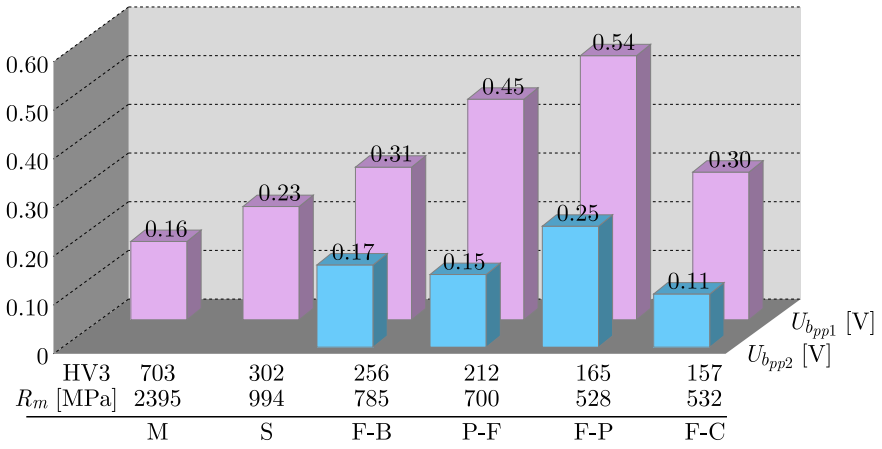

Fig. 3. The first peak $U_{b_{pp1}}$ and the second peak $U_{b_{pp2}}$ of rms Barkhausen envelopes for different steel grades

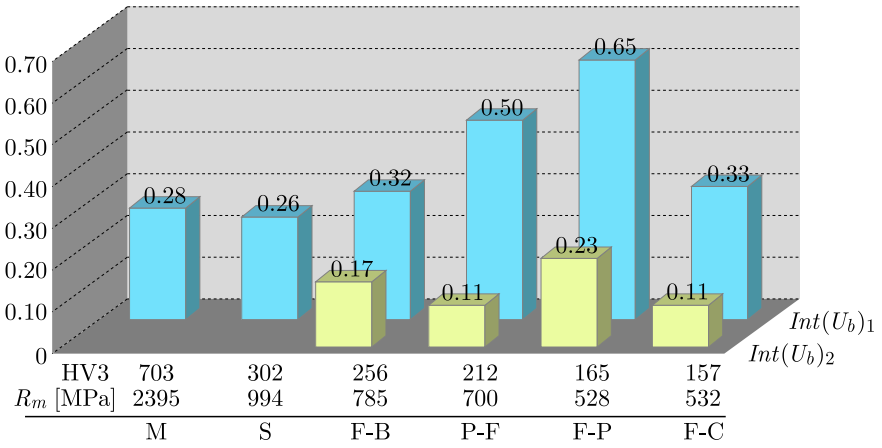

Fig. 4. Integrals of the half-period voltage signal of MBN ($Int(U_b)_1$ and $Int(U_b)_2$)

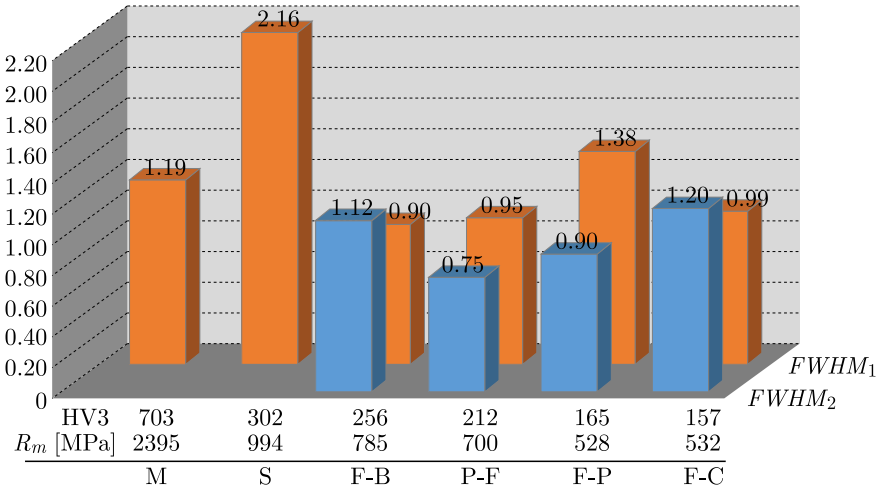

Fig. 5. Width of the first and second peaks determined from the rms envelope of the Barkhausen noise of the tested steel grades ($FWHM_1$ and $FWHM_2$)

Table 2 presents the HV3 hardness results of steel grades, whereas Table 3 shows parameters determined based on the metallographic and mechanical tests: d_{av} – grain size diameter and R_m – ultimate tensile stress. It was observed, that the values of mechanical parameters increase with the reduction of the amplitude and integral value determined from the envelope of BN.

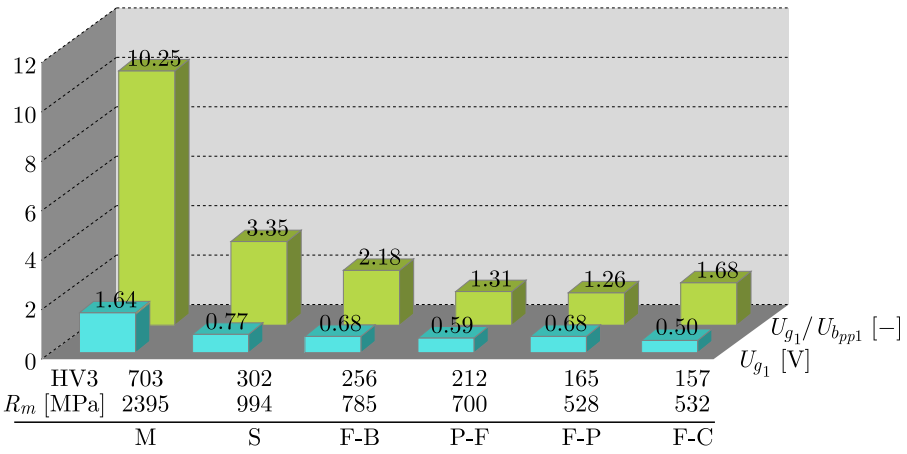

Fig. 6. Graphical representation of U_{g1} and $U_{g1}/U_{b_{pp1}}$ parameters for different steel grades

Table 3. Microstructural and mechanical properties of the steel grades tested

Steel grade	Mars 300	40NiCrMo7	S700MC	C55	S355	C15
Hardness [HV3]	703	302	256	212	165	157
Ultimate tensile stress R_m [MPa]	2396*	994	785	700	528	532
d_{av} [μm]	15.5	10.4	ferrite$_{(F)}$ 2.23 bainite$_{(H)}$ 1.77	pearlite$_{(F)}$ 16.06 ferrite$_{(F)}$ 15.75	ferrite$_{(F)}$ 3.88 pearlite$_{(F)}$ 1.12	22.2

* Fras *et al.* (2018)

As it is shown in Fig. 2, the MBN envelopes are characterized by a varied shape and variable number of peaks. In terms of the mechanical parameters, the Mars 300 has the highest hardness and tensile strength. On the BN envelope, one can indicate a single maximum reflecting the martensitic microstructure (M). The MBN amplitude of this steel has the lowest value due to the high dislocation density in martensite needles, which is typical for this structure (Honkanen *et al.*, 2021). In (Honkanen *et al.*, 2021) it was proved by means of the transmission microscope in the Lorentz mode that the domain walls anchor and bend on dislocations.

Specimen No. 2 has also a high-tempered martensite structure named also as sorbite (S). It contains small cementite particles in the fine grained ferritic matrix. Since the distribution of cementite in the ferritic matrix is practically homogeneous, only a single maximum is observed here. The dense distributed cementite particles can be treated as significant obstacles for movements of the domain walls and, as a consequence, this specimen is characterized by the Ub_{pp} parameter equal to 0.23 V. In (Tavares *et al.*, 2019), the anchorage of domain walls in sorbite steel on carbide precipitates was clearly illustrated. These precipitates were the major obstacles for movement of the domain walls in the microstructure with high-tempered martensite.

The S700MC steel (Specimen No. 3) represented a ferritic-bainitic microstructure. In that case, the MBN envelope had two maxima. The peaks are mainly attributed to nucleation and growth of new domains at various specimen defects and grain boundaries as well as the domain walls annihilation process. It has to be emphasized that the number of peaks depends on the number of phases in the material. The first peak obtained for a lower positive U_g was associated with the presence of ferrite in the microstructure, while the second one, for a higher U_g, was attributed to bainite.

Since the number of dislocations in ferrite grains is relatively low (Honkanen *et al.*, 2019), the domain walls can move more freely and with a higher speed. As a consequence, their anchoring takes place mainly at the boundaries of ferrite grains. Such feature is reflected in magnetic

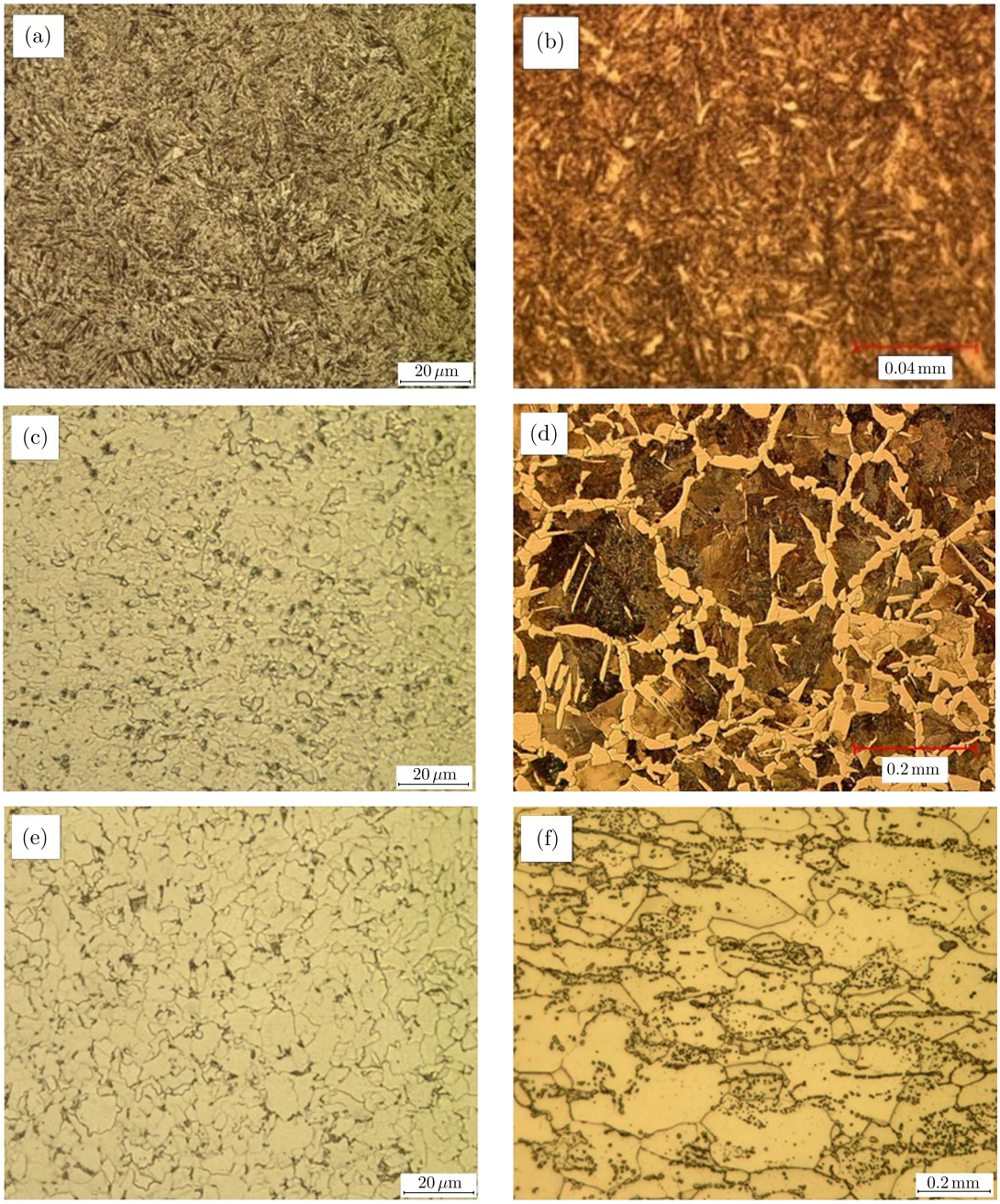

Fig. 7. Microstructures of different steel grades: (a) Mars 300 with the martensitic microstructure, $d_{qv\,M)} = 15.5\,\mu$m, 703 HV3, (b) 40NiCrMo4 with the sorbite microstructure (high-tempered martensite), $d_{av\,(S)} = 10.4\,\mu$m, 302 HV3, (c) S700MC with the ferritic-bainitic microstructure, $d_{av\,(F)} = 2.23\,\mu$m, $d_{av\,(B)} = 1.77\,\mu$m, 256 HV3, (d) C55 with the pearlitic-ferritic microstructure, $d_{av\,(F)} = 15.75\,\mu$m, $d_{av\,(P)} = 16.06\,\mu$m, $V_F = 31.2\%$, $V_P = 68.8\%$, 212 HV3, (e) S355 with the ferritic-pearlitic microstructure, $V_F = 87.9\%$, $V_P = 12.1\%$, $d_{av\,(F)} = 3.88\,\mu$m, 165 HV3, (f) C15 with the ferritic microstructure and secondary cementite precipitates, $d_{av\,(F)} = 22.2\,\mu$m, $d_{av\,(C)} = 0.9 \cdot 10^{-3}\,\mu$m, $V_F = 90.2\%$, $V_C = 9.8\%$, 157 HV3

investigations by a higher maximum than that in the case of Specimen No. 2. By contrast, the peak related to bainite is lower than that from sorbite (high-tempered martensite) in Specimen No. 2 and similar to the peak related to martensite in Specimen No. 1. The domain walls in bainite move more freely and their speed is greater due to the ferritic matrix of bainite, in which,

on the other hand, there are carbides that increase the number of Barkhausen jumps (anchor and disanchor domain walls).

Envelopes determined for Specimens 4 and 5 represent the pearlitic-ferritic and ferritic--pearlitic microstructure, respectively. These specimens differ in the phase volume and grain size. Honkanen *et al.* (2021) studied how domain walls moved in ferrite and pearlite. A movement of the domain walls in steels containing such phases begins in ferrite due to a not sufficient number of pinning sites in its grains. However, there are some hindering elements for domain walls movements in the form of ferrite-ferrite grain boundaries. The generator voltage responsible for the domain walls movement across the ferrite-ferrite grain boundaries is not sufficient to unlock the anchored domain walls at the ferrite-perlite grain boundaries. Only an increase in strength of the magnetic field causes a displacement of the domain walls located perpendicularly to the alternately arranged ferrite and cementite plates. It has been observed that the domain walls anchor or disanchor on the cementite plates during their movement (Honkanen *et al.*, 2021).

Specimen 6 has a lower amplitude than Specimen 5. According to (Gür, 2017), the presence of spheroidite in the ferrite matrix should increase the BN level due to pearlite areas in the ferrite matrix. However, the grain size serves as the main factor affecting the BN level. Based on the relation $Ub_{pp} \sim d^{\sim 0.43}$, it was found by Ng *et al.* (2003) that the BN amplitude decreases as the grain size increases. This is due to a less number of grain boundaries acting as the pinning sites. Ranjan *et al.* (1987) found for technical nickel, that the amount of grain boundaries could be treated as the dominant microstructural parameter affecting the magnetic properties. They discovered that the Barkhausen signal decreased with a grain size increase. Such results were confirmed by tests carried out on a low carbon steel (Anglada-Rivera *et al.*, 2001). Cumulative diagrams of grain size variation as a function of the BN level $U_{b_{pp1}}$ for metastable and stable phases are shown in Figs. 8-9. The metastable phases that represent non-diffusive/semi-diffusion products create dislocation clusters and, moreover, serve as a source of stress concentration during rapid cooling. The just mentioned factors, besides grain boundaries and precipitations, have an additional impact on the level of the BN signal. Figure 8a shows that if the level of the BN signal decreases, then the grain size-increases. A similar effect can be observed in Fig. 8b for cooled steels with phases being products of diffusion transformations, according to the Fe-C system. In the case of the ferritic-bainitic S700MC steel, the value for bainitic (metastable) phase was substituted for $U_{b_{pp1}}$. The results of stereological analysis are given in Table 2.

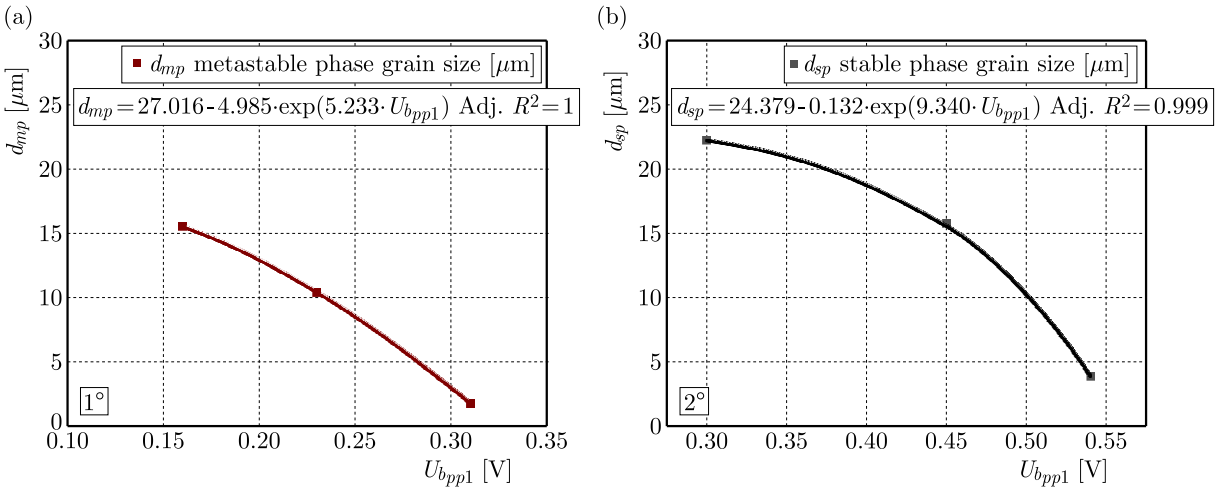

Fig. 8. Grain size as a function of the BN signal level $U_{b_{pp1}}$ for steels with phases being products of: (a) non-diffusion and semi-diffusion transformations, (b) diffusion transformations, according to the Fe-C system

It was observed that the background level of Barkhausen noise also changes depending on the microstructure of steel. It was noted that the background level of Barkhausen noise is lower when more pinning sites hindering movement of the domain walls in the tested material occur.

It was also found that high values of the $U_{g1}/U_{b_{pp1}}$ parameter indicates a very high hardness and tensile strength. In contrary to that result, a lower values of $U_{g1}/U_{b_{pp1}}$ parameters indicate lower values of the hardness and tensile strength, see Fig. 6. Changes in the parameter U_{g1} are not so clear, Fig. 6. However, similarly to the parameter $U_{g1}/U_{b_{pp1}}$, the highest U_{g1} values were observed for the highest hardness and tensile strength and, oppositely, the lowest U_{g1} values were obtained for the lowest hardness and tensile strength.

The results obtained from tests carried out on Specimens No. 1-6 meet the technical requirements for selected automotive and military structural elements. The microstructure and hardness values are in agreement with those recommended by the standards "T-ITS/5/13-CBM Technical condition. Steering rods, wishbones, torque rods and stabilizer rods as well as connectors of the suspension system of motor vehicles. Safety requirements and tests" (in Polish) and "T-ITS/63/13-CBM Technical condition. Ball joints of the steering and suspension systems of motor vehicles. Safety requirements and tests" (in Polish).

The parameters selected from Figs. 3, 5 and 6 created the basis for determination of a new parameter called the Modified Barkhausen Signal (MBS). It is characterized by the equation: $\mathrm{MBS} = (U_{g1}/U_{b_{pp1}}) + U_{g2} - FWHM_2$.

It was observed that the material hardness varied linearly as a function of the MBS parameter, see Fig. 9. This relationship became the basis for a model development enabling determination of mechanical properties, microstructure and grain size of the material. Since the hardness can also be treated as a measure of a microstructure that enables distinction between microstructures tested, it is possible to simultaneously assess either microstructure or mechanical properties using the MBS parameter.

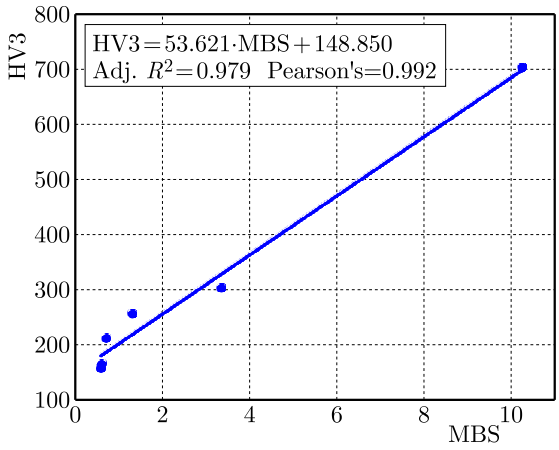

Fig. 9. Relationship between the hardness and MBS parameter

Moreover, if the value of the MBS parameter is greater than 1.3, the grain size of the material is determined using the $U_{b_{pp1}}$ parameter based on the relationship presented in Fig. 8a, whereas if the value of the MBS parameter is less than 1.3, the grain size can be evaluated based on the relationship presented in Fig. 8b, see Fig. 10.

4. Conclusion remarks

In this paper, a non-destructive method is proposed as an optional method for identification of the microstructure and mechanical properties of steel, based on BN measurements. The rms

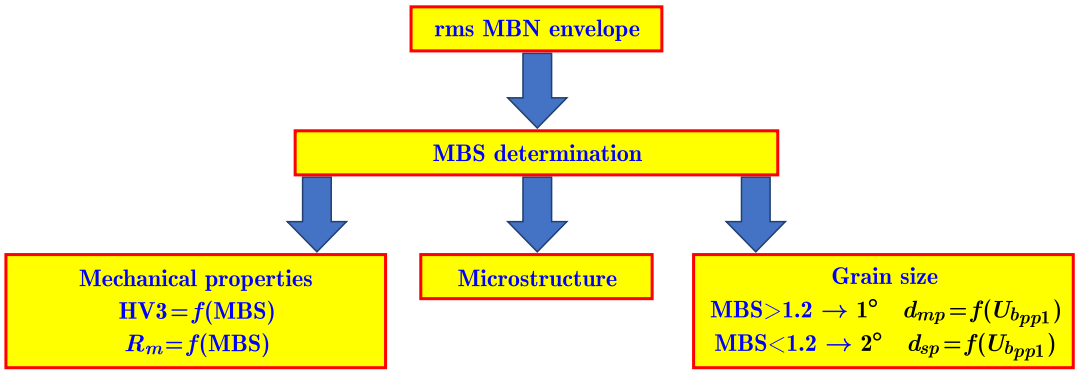

Fig. 10. Barkhausen noise procedure for predicting mechanical properties, microstructure and grain size of structural steels

amplitude of BN enables one to identify the number of phases in the material in question. The MBN double peak reveals two magnetic features and two phases in the specimen. A level of the BN signal depends on the microstructure and material grain size. Evaluation of the material microstructure can be done on the basis of the shape of MBN envelope as well as two parameters determined from the envelope: $U_{b_{pp1}}$ and U_{g1}. Based on the results for Specimen No. 6 representing ferritic structure with cementite precipitations, one can conclude that both parameters better describe the matrix of the material. This due to the fact that in ferrite, a displacement of the domain walls takes place between the adjacent grain boundaries. The parameter $U_{b_{pp1}}$ depends not only on the grain boundaries, but also on precipitations and dislocations. As a consequence, it expresses the microstructural features in the material matrix, whereas the parameter U_{g1} refers to strength of the magnetic field that is needed to overcome pinning obstacles by domain walls. The U_{g1} parameter can be applied to identify coexisting phases with the ferritic structure, i.e.: bainite, cementite or perlite.

The tests carried out can be treated as preliminary studies, and there is no doubt that the further research should be extended to a wider group of steels with an even more diverse structure and grain size. It was also observed that the increase of grain size reduced the level of Barkhausen noise for steels with structures that were products of both diffusion/semi-diffusion and diffusion transformation. Attention is also paid to the $U_{g1}/U_{b_{pp1}}$ parameter whose variation describes changes in the hardness and tensile strength.

A simple Barkhausen noise model is proposed using new magnetic parameters. It enables simultaneous assessment of mechanical properties, microstructure and grain size of the steel tested.

One can indicate BN as a method with a wide application potential in material investigations, especially after their production processes realised.

Acknowledgment

This work was co-financed by Military University of Technology under research project UGB 22-742/2024.

References

1. Anglada-Rivera L.R., Padovese L.R., Capó-Sánchez J., 2001, Magnetic Barkhausen noise and hysteresis loop in commercial carbon steel: influence of applied tensile stress and grain size, *Journal of Magnetism and Magnetic Materials*, **231**, 299-306

2. Astudillo M.R.C., Núñez N.M., Pumarega M.I.L., Ferrari G., Ruzzante J., Gómez M., 2022, Study of martensite induced by deformation with Magnetic Barkhausen Noise technique, *Journal of Magnetism and Magnetic Materials*, **556**, 1-12

3. Augustyniak B., 2003, *Magnetoelastic Phenomena and their Use in Non-Destructive Testing of Materials* (in Polish), Wydawnictwo Politechniki Gdańskiej

4. Blaow M., Evans J.T., Shaw B.A., 2005, Magnetic Barkhausen noise: influence of microstructure and deformation in bending, *Acta Materialia*, **53**, 2, 279-287

5. Błażewski S., Mikoszewski J., 1981, *Measurements of Metal Hardness* (in Polish), WNT

6. Cullity B.D., Graham C.D., 2009, *Introduction to Magnetic Materials*, Wiley

7. Fras T., Roth C.C., Mohr D., 2018, Fracture of high-strength armour steel under impact loading, *International —Journal of Impact Engineering*, **111**, 147-164

8. Gür C.H., 2017, Nondestructive monitoring of pearlite degradation in medium carbon steels, *The 14th International Conference of the Slovenian Society for Non-Destructive Testing*, Bernardin, Slovenia

9. Honkanen M., Santa-Aho S., Laurson L., Eslahi N., Foi A., Vippola M., 2021, Mimicking Barkhausen noise measurement by in-situ transmission electron microscopy – effect of microstructural on Barkhausen noise, *Acta Materialia*, **221**, 1-11

10. Huallpa E., de Montevade E.F., Capó Sánchez J.C., Campos M.A., Padovese L., Goldstein H., 2016, Use of Magnetic Barkhausen Noise (MBN) to follow up the formation of sigma phase in Saf2205 (UNS S31803) Duplex Stainless Steel, *Materials Research*, **19**, 5, 1008-1016

11. Hwang D.G., Kim C.G., Lee K.H., Kim H.C., 1993, The retarding field model of Barkhausen noise and permeability in conventional and highly grain-oriented 3% Si-Fe polycrystals, *Journal of Magnetism and Magnetic Materials*, **125**, 1-2, 129-137

12. Ivanova Y., 2022, Investigation of heat-treated steels using the magnetic noise method, *International Scientific Journal "Machines. Technologies. Materials"*, **16**, 4, 138-141

13. Jiles D., 1998, *Introduction to Magnetism and Magnetic Materials*, Taylor and Francis Group

14. Kaplan M., Gür C.H., Erdogan M., 2007, Characterization of dual-phase steels using magnetic Barkhausen noise technique, *Journal of Nondestructive Evaluation*, **26**, 79-87

15. Kleber X., Vincent A., 2004, On the role of residual internal stresses and dislocations on Barkhausen noise in plastically deformed steel, *NDT and E International*, **37**, 439-445

16. Makowska K., Kowalewski Z.L., 2020, Variation of Barkhausen noise, magnetic and crystal structure of ferromagnetic medium-carbon steel after different loading processes. *The Physics of Metals and Metallography*, **121**, 2, 115-122

17. Nebair H., Helifa B., Bensaid S., Zidelmen S., Lefkaier I.K., 2022, Martensite morphology and volume fraction evaluation of dual-phase X70 steel using magnetic Barkhausen noise technique, *Journal of Magnetism and Magnetic Materials*, **555**, 1-9

18. Neslušan M., Pitoňak M., Minárik P., Tkáč M., Koll ar P., Životský O., 2023, Influence of domain walls thickness, density and alignment on Barkhausen noise emission in low alloyed steels, *Scientific Reports*, **13**, 1-12

19. Ng D.H.L., Cho K.S., Wong M.L., Chan S.L.I., Ma X.-Y., Lo C.C.H., 2003, Study of microstructure, mechanical properties, and magnetization process in low carbon steel bars by Barkhausen emission, *Materials Science and Engineering: A*, **358**, 186-198

20. Pickering F.B., 1976, Physical metallurgy of stainless steel developments, *International Metals Reviews*, **211**, 227-268

21. Ranjan R., Jiles D.C., Buck O., Thompson, R.B., 1987, Grain size measurement using magnetic and acoustic Barkhausen noise, *Journal of Applied Physics*, **61**, 3199-3201

22. Sahebalm A., Kashefi M., Kahrobaee S., 2014, Comparative study of eddy current and Barkhausen noise methods in microstructural assessment of heat treated steel parts, *Nondestructive Testing and Evaluation*, **29**, 3, 208-218

23. Singh S.S., Awale A.S., Chaudhari A., Nahak B., 2020, Monitoring the microstructural changes of heat treated medium carbon steel by Barkhausen noise and hysteresis loop techniques, *Materials Today: Proceedings*, **26**, 1198-1202

24. Tavares S.S.M., Noris L.F., Pardal J.M., Silva da M.R., 2019, Temper embrittlement of supermartensitic stainless steel and non-destructive inspection by magnetic Barkhausen noise, *Engineering Failure Analysis*, **100**, 322-328

25. Zhu B., Xu Z., Wang K., Zhang Y., 2020, Nondestructive evaluation of hot stamping boron steel with martensite/bainite mixed microstructures based on magnetic Barkhausen noise detection, *Journal of Magnetism and Magnetic Materials*, **503**, 53, 1-8

Manuscript received November 7, 2023; accepted for print January 8, 2024